Fuel 352 (2023) 129145

Contents lists available at ScienceDirect

Fuel

journal homepage: www.elsevier.com/locate/fuel

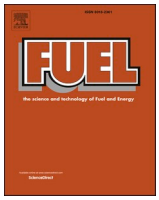

Full Length Article

Towards fuels production by a catalytic pyrolysis of a real mixture of post-consumer plastic waste

M.F. Paucar-Sánchez, M.A. Martín-Lara, M. Calero, G. Blázquez *, R.R. Solís, M.J. Muñoz-Batista *

Department of Chemical Engineering, University of Granada, Avda. Fuentenueva s/n, Granada, Spain

ARTICLE INFO

Keywords:
Pyrolysis
Plastic wastes
Sepiolite
Montmorillonite
Fuels

ABSTRACT

The contribution provides a valorization alternative for rejected plastic wastes from mechanical-biological treatment (non-recyclable material) *via* an in-situ catalytic pyrolysis process focused on the production of a liquid fraction with similar properties to traditional fuels (i.e., gasoline, kerosine, and diesel). According to the ASTM recommendations, on small samples without prior physical separation, fuel fraction identification was carried out by Simulated Distillation along with a hydrocarbon types analysis and complemented with CHNS-O analysis and Fourier Transform Infrared Spectroscopy. Two catalytic structures were employed named Sepiolite and Montmorillonites, both *K*10 and K30, which after simple heat treatment to stabilize the structure, were characterized to analyze the main properties affecting the catalytic activity and product yields (i.e., morphological and acidity properties). A whole screaming of the products by analogy with hydrocarbon of the petroleum industry is presented. Such an approach allows a real evaluation of the studied technology in the current energy scenario.

1. Introduction

Plastics have played a crucial role in industrial development over the past 50 years, serving as a main component in a wide range of applications in various sectors. These applications encompass packaging, construction, healthcare, electrical devices, among many others. [1–3]. The plastic demand has been steadily enhanced, which has resulted in a tremendous increase in plastic waste generation. The reuse of plastic components should be the first alternative, but it is limited by deterioration after its useful lifetime. In addition, a very competitive cost adjustment for plastic production keeps down the proper development of this environmentally friendly scheme. On the other hand, the increased recycling of waste-related plastic is limited by several technical and economic bottlenecks [4]. It is even more complicated with some plastic-based components such as multi-element products (e.g. plastic-metallic or plastic-inorganic structures), multi-layer materials, or polymeric components including toxic compounds (e.g. additives like brominated flame retardants, phthalates) [2]. Besides, a lot of plastic waste is non-recyclable by traditional methods, such as e.g., that comes from rejected fractions of mechanical biological treatments. In this context, the development of valorization alternatives such as thermal and catalytic pyrolysis, gasification, and plasma are emerging as potential alternatives [1,2,3].

In particular, the pyrolysis process can convert the plastic waste into three fractions named liquid (which may have fuel properties) [5,6,7], solid (a char with a carbonaceous structure and potential applications as adsorbents or catalytic supports) [8,9,10], and gases (with a high calorific value equivalent to natural gas ~ 44 MJ/kg) at temperatures above 300 °C through thermal decomposition of the polymer structure [1,11,3]. Although, in general, pure pyrolysis is not a highly selective process, pyrolysis schemes are relatively flexible due to main operating conditions that can be manipulated to optimize product yields [3,12]. The catalytic alternative tries to solve some of the limitations of the traditional pyrolytic process. Several contributions under pure pyrolysis conditions of plastic-containing materials describe the presence of impurities in the liquid oil and low yields, which can be adjusted using a well-designed catalytic pyrolysis scheme [1,3]. Catalytic schemes also intend to reduce the inherent temperature dependence of the process by working at considerably low temperatures and including other catalytic-related parameters in the scheme which define the efficiency of the whole process. Surface area and pore distribution size, as the acidity (total and strength type), are some critical features of the employed

* Corresponding authors.
E-mail addresses: gblazque@ugr.es (G. Blázquez), mariomunoz@ugr.es (M.J. Muñoz-Batista).

https://doi.org/10.1016/j.fuel.2023.129145
Received 9 March 2023; Received in revised form 29 May 2023; Accepted 28 June 2023
Available online 4 July 2023

catalysts [13,14]. Thus, many catalytic materials have been applied to produce the gases, liquids, and chars with appropriate characteristics and high purity. It is well-described that, in general, catalytic schemes promote an enhancement of the gas yield and reduce the amount of the liquid fraction, which results in lighter hydrocarbon distributions. However, this liquid reduction can be compensated by a clear quality improvement, producing mixtures with greater commercial interest like gasoline, diesel, or jet fuel products. Zeolite catalysts have been extensively studied. For plastic-to-fuel applications, a few examples can be highlighted. HZSM-5, HY, HMOR, and HUSY with a dominated micropores structure, MCM-41, and SBA-15 as mesoporous catalysts are well-analyzed [14]. Traditional catalytic samples such as metal oxides, alkali carbonates, and metal complexes have been mainly used to improve the monomer recovery [14]. Several clays have emerged as competitive alternatives by reducing process costs. Montmorillonites and their analogies (i.e. saponite, hectorite, beidellite), although usually less active than zeolites below 600 K, have proven in many cases to be more efficient in processes at high working temperatures [14,15]. The catalytic response is also strongly related to the configuration of experimental scheme setups. Two schemes have usually been reported, taking into account the interaction of the catalyst with the starting raw material or generated pyrolytic vapors, as in-situ or ex-situ catalytic pyrolysis. In-situ catalytic pyrolysis is developed using a well-defined one-step in which the catalyst is mixed with the raw material to be pyrolyzed. Instead, ex-situ catalytic pyrolysis occurs when raw materials are pyrolyzed to generate vapors that will be transferred to a catalytic reactor (two steps) [16].

This contribution presents the development of a pyrolysis process for non-recyclable plastics, utilizing an in-situ catalytic scheme employing Sepiolite and two Montmorillonites (MK10 and MK30) as catalysts, with the objective of producing fuels. Through a rigorous analysis of Simulated Distillation and product characterization based on hydrocarbon types, conducted on small samples without prior physical separation or distillation, our aim is to provide a comprehensive understanding of the proposed technology while establishing a parallel with conventional fuels generated by the petroleum industry. Our approach enables a critical evaluation of the resulting products for immediate applicability within the current fuel sector.

2. Materials and methods

2.1. Raw material

The plastic waste materials come from the rejected plastic fractions of Granada's mechanical biological treatment (MBT) plant (Spain) and following a well-defined scheme including ramdom selection and basic characterization as described in the Supplementary material document. The mixture was composed of rigid polypropylene (PP), expanded polystyrene (EPS), high impact polystyrene (HIPS), polypropylene film (PP film), and polyethylene film (PE film). These were previously separated, washed, dried, and subjected to a size reduction process (1–3 mm) to facilitate homogeneity in the pyrolysis test. The average composition of the raw material received showed 56.10% of PP, 12.65% of PP film, 12.65% of PE film, 10.05% of EPS, and 8.55% of HIPS.

2.2. Preparation and characterization of the catalysts

Sepiolite (SE) and Montmorillonites K10 (MK10) and K30 (MK30) were supplied by Sigma Alrich. The chemical, structural, and morphological properties were stabilized by calcination at 550 °C under atmospheric pressure with air for 3.5 h in a Nabertherm, L 3/11/B180 Model furnace muffle and conserved in a desiccator. The morphological modifications were analyzed in a Micromeritics ASAP2429 Porosity Analyzer according to ASTM D3663 and ASTM D4365 designations [17,18]. At the same time, the pore size distributions were calculated by ASTM D4641 standard [19]. The strength of active sites measurement on the surface of catalytic materials was carried out by temperature-programmed ammonia desorption under helium flow (50 mL/min) from room to 500 °C with 30 °C/min heating gradient over approximately 0.085 g of sample on a chemisorption analyzer AutoChem II 2920 model from Micrometrics Instrument Corporation provided with a Thermal Conductivity Detector. Before the chemosorption, the samples were pretreated at 450 °C under He flows for one hour and then cooled to room temperature. Chemisorption was performed using a mixture of ammonia and helium at 10% (v/v) for 20 min.

2.3. Pyrolysis reactor and operation conditions

The plastic waste pyrolysis experiments were carried out on a fixed horizontal laboratory-scales reactor made of stainless steel 316 (internal diameter: 4 cm and length: 34.25 cm) inserted in a Nebertherm R 50/250/12 Model furnace. A flowmeter and a chiller were integrated to regulate the inert drag gas flow and cracked gas cooling (see Fig. 1).

20 g of sample with 1 and 2 g of catalytic material, uniformly spread over the plastics blend, were collocated in a closed 316 stainless steel tubular vessel (internal diameter: 27.25 mm and length: 30.6 cm) with a chimney hole and heated to a rate of 10 °C/min from room temperature to 500 °C, which was kept by 60 min more with a constant flow rate of 0.8 L/min of nitrogen. Then, the reactor was cooled to room temperature under a permanent nitrogen purge. A cooling bath separated liquid and gas products at −7 °C. The liquids were collected in an ore-weighted glass vessel, while the gases were in a TEDLAR gas sampling bag every fifteen minutes. The sampling TEDLAR bags were filled for 2.5 min (2 L).

Solid residue and oil product were directly measured then the yields were calculated according to the following equations (gas yield by difference):

$$\eta_l = \frac{m_l}{m_m}.100 \quad (1)$$

$$\eta_s = \frac{m_s}{m_m}.100 \quad (2)$$

$$\eta_g = 100 - (\eta_l + \eta_s) \quad (3)$$

where m_m, , m_l and m_s are the weights of the plastic sample, liquid, and solid products, respectively, and η_l, η_s and η_g are the yields of liquid, solid, and gases, respectively. The solids included char and coke.

2.4. Gases analysis

Non-condensed hydrocarbons and gases were identified on a Micro GC Agilent 990 Bio-Gas analyzer with two channels and thermal conductivity detectors (TCD). Two Agilent J&W Molesieve (5 Å zeolite molecular sieve with 20 m length and inner diameter of 0.25 mm and a

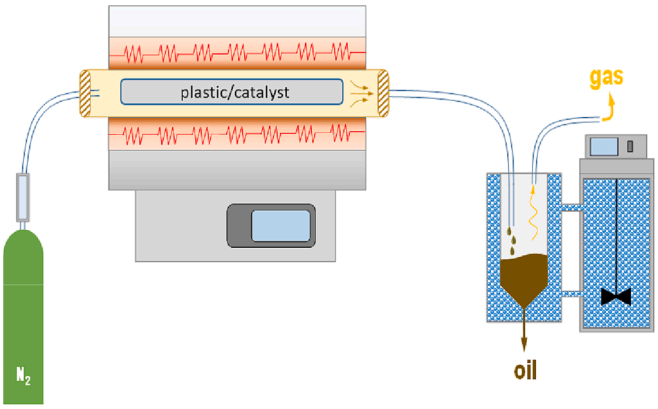

Fig. 1. Schematic representation of the pyrolysis setup.

film unit of 30 μm) and PoraPLOT Q (Polystyrene-divinylbenzene with 10 m length and inner diameter of 0.25 mm and 8 μm of film thickness) capillary columns were used. The operating conditions included backflushes, an injector temperature of 110 °C, and the oven at an isothermal temperature of 80 °C with pressures of 200 and 150 kPa, respectively, at constant helium flow. The samples were injected directly from TEDLAR bags.

2.5. Liquid analysis

2.5.1. Elemental analysis

Elemental analysis of the pyrolytic and catalyzed oils was carried out in a Thermo Scientific Flash 2000 CHNS-O Analyzer by rapid combustion with pure oxygen. The gases pass across a chromatographic separation column and a thermal conductivity detector to the ASTM D5291 designation [20].

2.5.2. Chemical constitution

A PerkinElmer Spectrum 65 of Infrared absorption spectroscopy by Fourier-Transform analysis was used to qualitatively identify organic and inorganic compounds by functional groups in non-catalyzed and catalyzed oils. The spectrums were recorded between the frequency range of 4000 and 550 cm^{-1} with a resolution of 1 cm^{-1}.

2.5.3. Simulated distillation (SD)

The boiling range of the pyrolytic and catalyzed oils, such as the petroleum derivatives, was determined on a PerkinElmer Clarus 590 Gas Chromatograph with a flame ionization detector (FID) according to the designation ASTM D2887 [21]. An ELITE 2887 capillary column with a cross bond of dimethylpolysiloxane of 10 m in length and 0.53 of inner diameter and 2.65 μm of the film was used. The liquid samples were injected directly, and no liquids reduced the viscosity with carbon disulfide. The assessment of potential products that could be recovered from oils was evaluated according to **Table S1** of fractions criteria [22].

2.5.4. ASTM D86 distillation from the fuels

Atmospheric distillation of liquid fuel products quantitatively determines the boiling range characteristics of light and middle distillates by performing a simple batch distillation. The volatility characteristics provide information about safety and performance, composition, properties, and behavior during the storage and use of the fuels. To evaluate the stream performance and fuel distillation specification requirements similar to what might be achieved in an atmospheric distillation unit, the streams' simulated distillations curves were calculated from the SD curve according to the boiling range [23] shown in **Table S2**, then converted to ASTM D86 distillation curves by 3A3.2 API procedure (**Tables S3** and **Table S4**) [24]. The overlapping areas between cuts were normalized to determine the decreasing cumulative fraction, then multiplied by their corresponding areas to add them to the uppercut and the difference to the lower stream.

2.5.5. Hydrocarbon types analysis

Hydrocarbon types were determined by mass spectroscopy based on the summation of characteristic mass fragments scanning specified in the methods ASTM D2789, ASTM D2425, ASTM D2786, and ASTM D3239 [25–27] for hydrocarbons boiling within the range C_5 to 205 °C (light fraction) and 205 to 540 °C (middle distillate plus bottoms). For this, a gas chromatograph Agilent 8860 model coupled to a triple-quadrupole Agilent 5977 model mass spectrometer detector with analysis scan speed $\leq$ 20000 Da/s and ionization energy by the electronic impact of 70 eV and provided by nonpolar phase ZB-5 ms (30 m, 0.25 mm internal diameter and 0.25 μm of fill thickness) Phenomenex capillary column was used. The oven was programmed with an initial temperature of 42 °C for 4 min, an injector temperature of 240 °C, and a final temperature of 320 °C for 4 min with a 6 °C/min gradient. The samples were weighed and diluted in 1 mL of chloroform and injected in split mode (5:1) at a constant flow of helium of 1 mL/min.

A suitable synthetic mixture of pure hydrocarbons encompassing the boiling range specified by the ASTM D2887 method [5] was analyzed previously to identify the range of the retention times of streams for analysis. The referential retention times of each stream were calculated according to the following linear regression:

$$RT_x = \left(\frac{RT_2 - RT_1}{BP_2 - BP_1}\right).(BP_x - BP_1) + RT_1 \quad (4)$$

where the boiling point and retention times of referential paraffins are represented by BP_1, BP_2, RT_1, and RT_2, while the boiling points and retention times of the compounds in the sample are doing by BP_x and RT_x.

Obtained the referential retention times, the concentration analysis of the total paraffins, monocycloparaffins, dicycloparaffins, alkylbenzenes, indans and tetralins, and naphthenes from naphtha were determined by the standard test method ASTM D2789 [25]. In contrast, the saturated hydrocarbon and aromatics types from kerosine and diesel were identified by the ASTM D2425 designation. At the same time, the bottoms were set out by the ASTM D2786 and ASTM D3239 standards [26,27,28]. The characteristic mass fragments were added to each stream according to its boiling range, considering the abovementioned overlapping criteria.

3. Results and discussion

3.1. Characterization of the catalysts

Fig. 2 **(A, B)** shows the N_2 adsorption–desorption isotherms and pore size distribution, respectively. According to the IUPAC classification of physisorption isotherms, all materials can be classified as type IV, accompanied by capillary condensation hysteresis loops of type H3 for sepiolite and type H4 for montmorillonites [29]. Table 1 summarizes the morphologic characteristics of the catalytic materials analyzed by N_2 adsorption–desorption isotherms after calcination. It is appreciable the absence of micropores in montmorillonite structures, a condition that is not changed from the raw state, as shown in Table 1 and **Table S5**; however, the calcinated ones have a decreased BET surface (7 to 9 percent), a total volume reduction of ca. 2.8%, and lessened average pore size of 7 to 12 percent, while, although calcinated sepiolite has a diminished BET (51.6%), micropore (93.7%), and external surfaces (9.8%), its total volume and average pore size increased by 30.8% and 5.1%, respectively. Despite the calcination, the surface area and pore volume of sepiolite displayed typical variations from the natural forms reported in the literature [30–31]. Conversely, montmorillonites exhibited close values [32–33]. As well known that acidic sites are the main active sites for the cracking effect over the surfaces of catalysts during catalytic pyrolysis processes [34], identified as weak (Brønsted acid) and strong (Lewis acid) sites on the studied samples; of these, both contributions both weak acid sites and moderate acid sites, were observed (Fig. 2C) [35–36]. However, a clear difference can be seen for catalytic samples with Sepiolite and Montmorillonite structures. MK10 and MK30 showed a well-defined peak centered at 170 °C, which can be associated with characteristics of weak acid sites, while the SE sample described a broad band caused by the contribution of weak acid sites, but with an important contribution from moderate acid sites according to the identification of the maximum intensity situated at 315 °C [35]. NH_3-TPD also allows calculating the total acidity at the surface of the catalysts. The acidity expressed as millimoles of NH_3 per gram reached a maximum for SE, followed by MK30 and MK10 (Table 1). As a result, stable acidic materials with a remarkable and defined mesoporous character, deduced from the porous size distribution, were obtained.

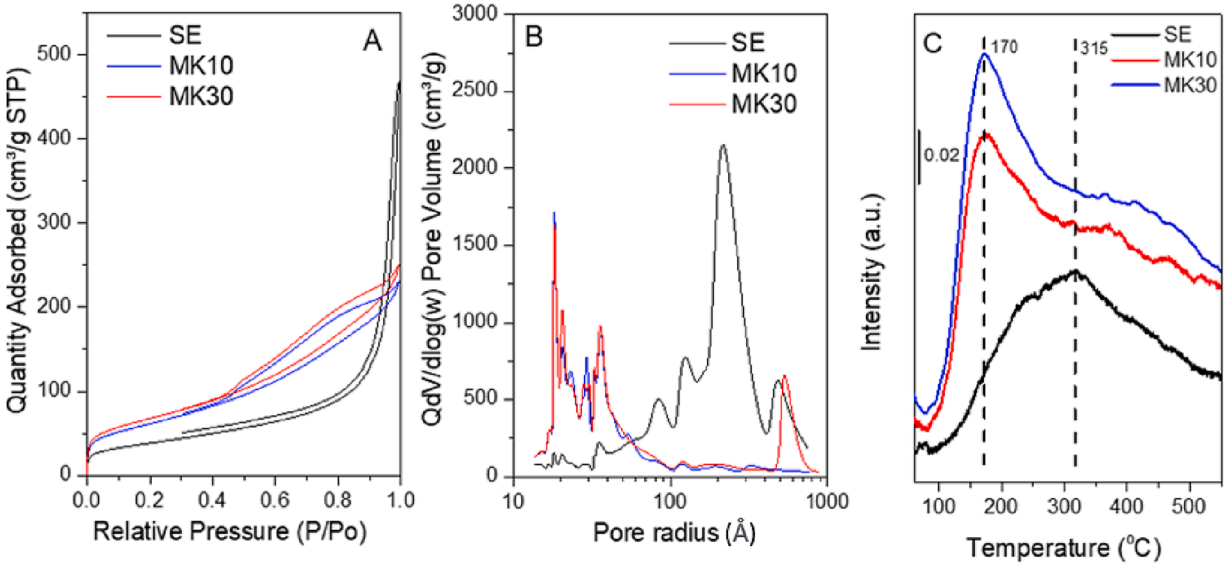

Fig. 2. Analysis of morphological and acidity properties of the samples (A) N_2 isotherms, (B) pore size distribution and (C) NH_3 temperature programmed desorption curves.

Table 1
Properties of the catalytic materials.

Catalyst	S_{BET} (m^2/g)	S_{MP} (m^2/g)	S_{EXT} (m^2/g)	V_T (cm^3/g)	V_{MP} (cm^3/g)	Average Pore Size (Å)	Acidity (mmol/g)
SE	138	9	129	0.726	0.004	82	0.290
MK10	224	–	224	0.357	–	55	0.233
MK30	245	–	245	0.389	–	54	0.276

3.2. Fraction yields and chemical composition

Table 2 shows the effect of sepiolite and montmorillonites on the average fraction yields obtained from the catalytic pyrolysis of the studied mixture of waste plastics in triplicate. As can be seen, an increase in gas fraction and a reduction in the amount of liquid were registered as a general trend. An enhancement of gases and a reduction of the liquid fraction when more catalytic material is added is also detected, while the solids showed wt. % between 6.6 and 8.1. The average values obtained led to a less than 5 % relative standard deviation.

As expected after treatments, MK10 and MK30 remain similar in morphological terms (Table 1 **and S5**); however, total acidity quantification provides some differences. As summarized in Table 1, the total acidity of the MK30 sample is relatively higher than the MK10 sample, approaching the values measured for the SE one, which, as aforementioned, has a higher contribution from moderate acid centers (above 300 °C). As morphologic and acidity remarkably influence on the selectivity, a ratio between total acidity/total superficial area is determined for each catalyst. This quantitative parameter allows a preliminary analysis of yield to the gas and liquid fraction. Such ratio, defined in Fig. 3A-D as Acidity/S_{BET} (millimoles of NH_3 per m^2 of the catalytic surface), allows identifying two clearly defined areas. MK10 and MK30 to lower ratios produce fewer amounts of gas and a higher liquid fraction, while SE provides a higher gas fraction. The described trend is also independent of the used catalyst percentage (5 or 10% wt.). The correlation of Fig. 3 suggests that the selectivity profile is preferably associated with the type of acid centers rather than the total acidity of the sample. Obviously, and as discussed below, the pore distribution of the samples must also be considered a relevant factor.

Table 2
Gas, liquid, and solid yield (wt.%).

Catalyst percentage in the waste plastic feed	Gas	Liquid	Solid
0%	36.69	56.70	6.61
5% SE	42.14	50.44	7.43
10% SE	44.20	48.50	7.30
5% MK10	39.00	54.26	6.74
10% MK10	40.70	52.62	6.68
5% MK30	37.57	54.32	8.11
10% MK30	38.69	53.57	7.74

The increase of solids percentage concerning the pyrolysis without catalytic materials could also be attributed to coking formation due to acid sites of catalytic material [37], in addition to the porosity effects because of transport limitations, mainly when bulky molecules are involved [38]. Microporous in SE, and mesoporous volume extra of MK30 in the 500 and 600 Å range concerning MK10 (Fig. 1B), suggest that coke formation is due to heavy compounds adsorbed and trapped in these as well as catalyst/waste-plastic relation by the coke reduction when more catalyst is added than the individual acidic strength of each one. Nevertheless, although the acidity of SE is higher than MK30, coke reduced production could be due to the Lewis centers associated with a small number of exchangeable cations' [39]. The gas composition, Fig. 4, shows that probably condensable gases (propane and butane) and liquid light fractions (pentane) produced by catalytic cracking are under the thermal cracking effect when these leave the liquid phase that contains the catalyst. Typical light hydrocarbon reactions show pentanes decomposition begins at 390 °C without dehydrogenation. Still, with increasing temperature, demethanization occurs along with deethanization and depropanation. At about 435 °C, butane usually decomposes into methane–propane, and ethane–ethylene. Propane has certain ethane formation, while the demethanization is approximately the same as the dehydrogenation [40]. The presence of carbon monoxide and carbon dioxides in gases may be due to the material's origin and traces of organic and inorganic impurities over plastics and additives used in their manufacturing [41].

Table 3 shows the liquid products derived from pyrolysis expressed in wt. %. Concerning uncracked, there was a little nitrogenating from 0.1 to 0.3% promoted probably by catalytic and thermal cracking intermediates of reaction generated as by-products, along with deoxygenation reactions from 51 to 83% when the lowest amount of catalyst was used. The presence of catalysts and their relative augment was favorable for the hydrogenation of liquid fraction from 9 to 22%,

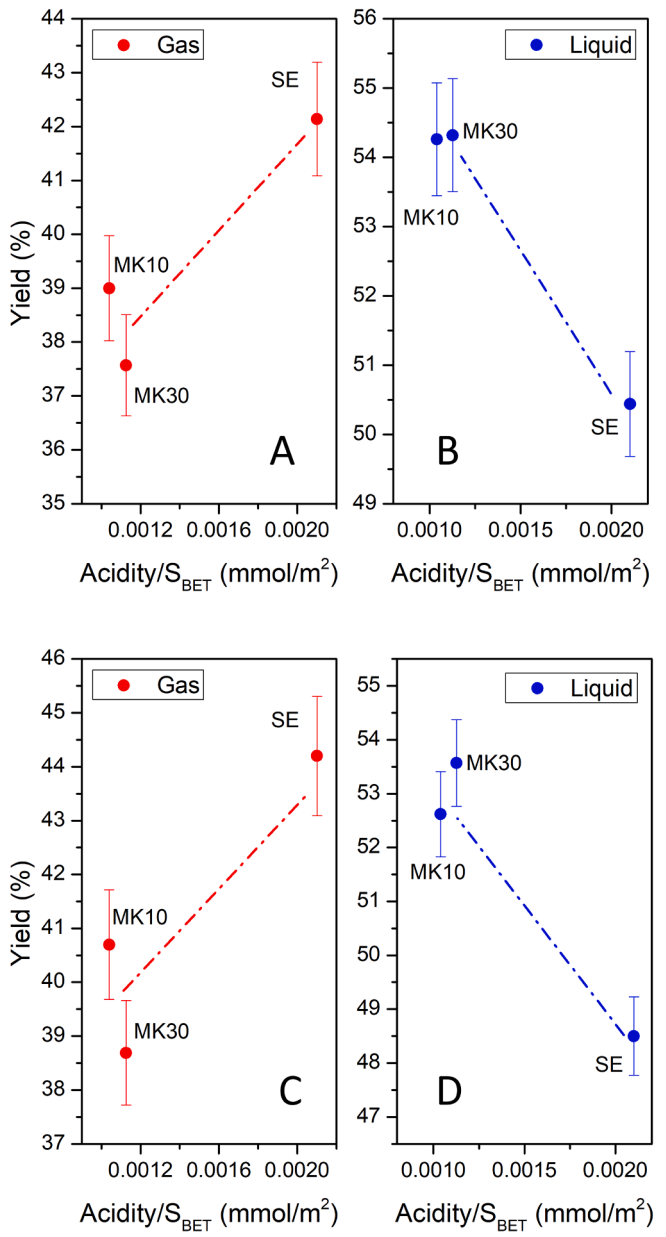

Fig. 3. Acidity/S_{BET} ratio as a function of the gas and liquid yield. (A) and (B) describe results obtained using 5 % of catalyst, and (C) and (D) the data using 10% of catalyst.

calculated by carbon–hydrogen relation, which increases the heating value [42]. The proportions of elements registered vary over reasonably narrow limits like conventional petroleum (Carbon: 83.4 ± 0.5%; Hydrogen: 10.4 ± 0.2%; Nitrogen: 0.4 ± 0.2% and Oxygen: 1.0 ± 0.2%) [43]; however, hydrogen content, from 41 to 56 % higher than petroleum, gives the obtained liquids a better heating value.

A structural group analysis of obtained liquid samples was realized by Fourier Transform Infrared Spectroscopy (FTIR) to provide detailed information about the chemical constitution of these oils. The FTIR peaks frequency range showed similarity for noncatalytic and catalytic cracked liquids with some differences in the absorbance values; according to Beer's Law, the variations in the absorbance intensity are proportional to the concentration [44]. The main peaks, shown in Fig. 5, are between 3080 and 3020 cm^{-1} (C-H medium stretch) for alkenes; 2960 – 2850 cm^{-1} (C-H strong stretch) for alkanes; 1760 – 1670 cm^{-1} (C = O strong stretch) for aldehydes, ketones, carboxylic acids, and esters; 1680 – 1640 cm^{-1} (C = C medium and weak stretch) for alkenes; 1650 – 1580 (N-H weak stretch) for amines; 1600 – 1500 cm^{-1} (C = C weak stretch) for aromatics rings; 1470 – 1350 cm^{-1} (variable scissoring and bending) for alkanes; 1340 – 1020 cm^{-1} (medium stretch) for amines; 1260 – 1000 cm^{-1} (strong stretch) for alcohols, ethers, carboxylic acids, and esters; 1000 – 675 cm^{-1} (C-H strong bend) for alkenes; 870 – 675 cm^{-1} (C-H strong bend) for phenyl ring substitution; and 700 – 610 cm^{-1} (C-H broad stretch) for alkynes [43]. Certain compounds could be attributed to the origin of plastic waste, its additives, and organic and inorganic impurities [45]. Although the drag nitrogen could form nitrogenated bonds, according to structure, these would influence pyrolytic oil instability as in the fuels obtained [46], in addition to the deposition of ammonium chlorine salts if exist traces of chlorine [47] by thermal cracking of PVC fragments. At the same time, oxygenated bonds would give particular acidity by naphthenic acid formation (linear, cyclic, and aromatic carboxylic groups) [48].

3.3. Simulated distillation and product yield

The simulated distillation curves of liquid products derived from thermal and catalytic cracking of the mixture of plastics are shown in Fig. 6. Results indicate that the volatilization temperature increased for liquid products from catalytic cracking because of changes in the distribution of products provocative by the rising gas yield of up to 20 % due to the thermal cracking of light compounds of the liquid fraction, which reduced from 4 to 11 %, and the presence of a more significant amount of high boiling cuts, that increased from 5 to 42 %. The displacement of the distillation curves to the left shows a naphtha reduction of up to 36 %, kerosene rising by 32 %, distillate fuel oil by 33 %, and light and heavy vacuum gas oils by 21 and 41 %, respectively, concerning the thermal cracking.

The distribution of the products is reported in Table 4. When more SE is added, kerosine increases by cracking distillate and vacuum gas oils. Light naphtha (coming from heavy naphtha cracking) absence could be due to this being broken into gases by the micropores' presence, which, regarding thermal cracking, augment from 15 to 20% in SE. The absence of micropores in MK10 reduces the cracking of heavy naphtha by about 8% compared to SE, and the little light naphtha formed is broken into gases. When MK10 increases, Light Vacuum Gas Oil (LVGO) and HVGO diminish to rise in light and heavy naphtha; light naphtha comes from medium naphtha, and a certain proportion is broken into gas. Unlike MK10, MK30 allows obtaining the highest amount of distillate Fuel Oil than other catalytic materials by breaking LVGO and HVGO, and more kerosine than MK10 and 5% SE, but with lesser heavy naphtha cut and cracking of the light naphtha present into gases. Adding more MK30, high boiling point cuts grow at the expense of light ones, and the little amount of light naphtha is transformed into gases.

3.4. Chemical composition of the products

3.4.1. Gasoline

For analogy with hydrocarbon present in petroleum, the analysis of light, medium, and heavy naphtha were made together as gasoline. Fig. 7 shows the ASTM D86 distillation curve for gasoline (**A**), its classification into paraffins, naphthenes, and aromatics (**B**), along with the categorization of hydrocarbon types in more detail (**C**). Some differences were observed in hydrocarbon group content according to the catalytic material used. The yield of paraffins, naphthenes, and aromatics varied when their amount increased, raising naphtha and paraffins by aromatics reduction; except on 10% MK10, where paraffins also reduced. At lower SE, the highest amount of alkylbenzenes formation was observed. For this reason, ASTM D86 distillations have higher boiling points than the gasoline obtained without a catalyst.

Saturated, the most chemically stable species, are present in gasoline from 20 to 80% (typically between 30 and 60 %) along with aromatic content to about 27 to 35 % to meet the emissions reduction requirements of the maximum permitted benzene (1%); aromatics have

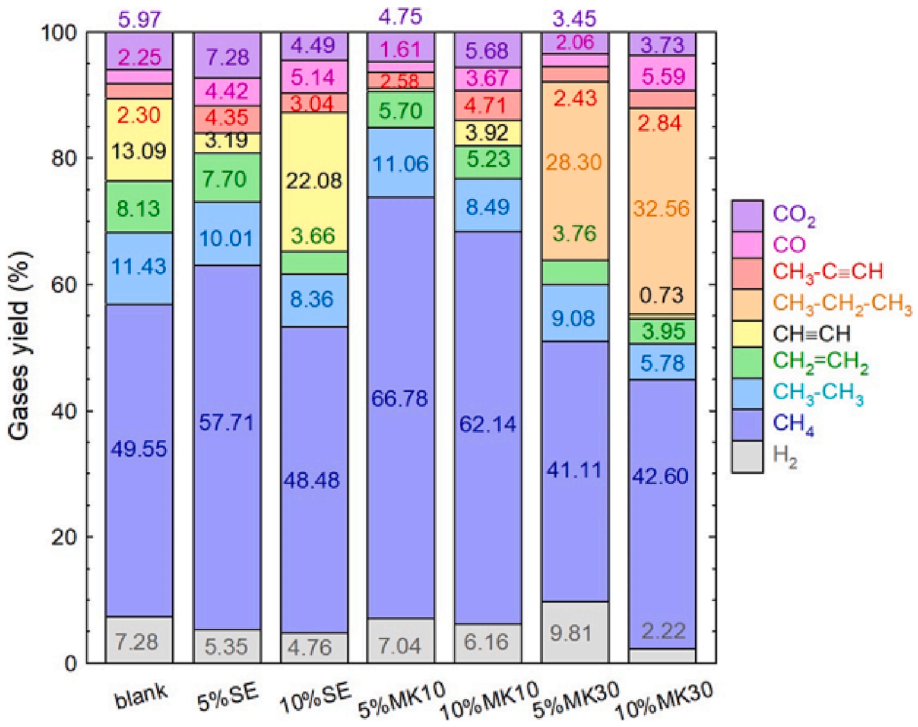

Fig. 4. Gases composition under catalytic conditions and non-catalytic reference. Experimental conditions: 20 g of sample; catalyst (if added), 1 g (5% mass) or 2 g (10% mass); heating rate, 10 °C/min, holding temperature, 500 °C; holding time, 60 min; N_2 flowrate 0.8 L/min.

Table 3
Elemental composition of the liquid fraction obtained by noncatalytic and catalytic cracking.

Catalyst percentage in the waste plastic feed	Nitrogen (wt.%)	Carbon (wt.%)	Hydrogen (wt.%)	Oxygen (wt.%)
0%	0.0	84.1	13.4	2.5
5% SE	0.1	82.8	15.8	1.3
10% SE	0.2	82.0	15.9	1.9
5% MK10	0.3	84.0	15.3	0.4
10% MK10	0.3	79.6	16.2	3.9
5% MK30	0.2	84.3	14.7	0.8
10% MK30	0.1	79.8	15.4	4.7

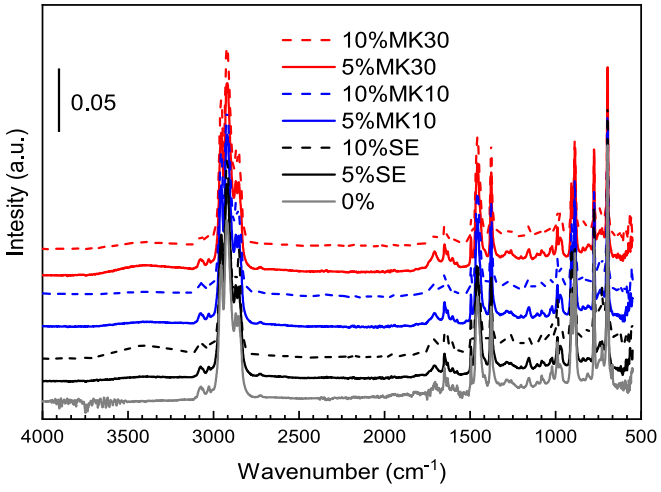

Fig. 5. FT-IR spectra of the liquid fractions derived from noncatalytic and catalytic cracking.

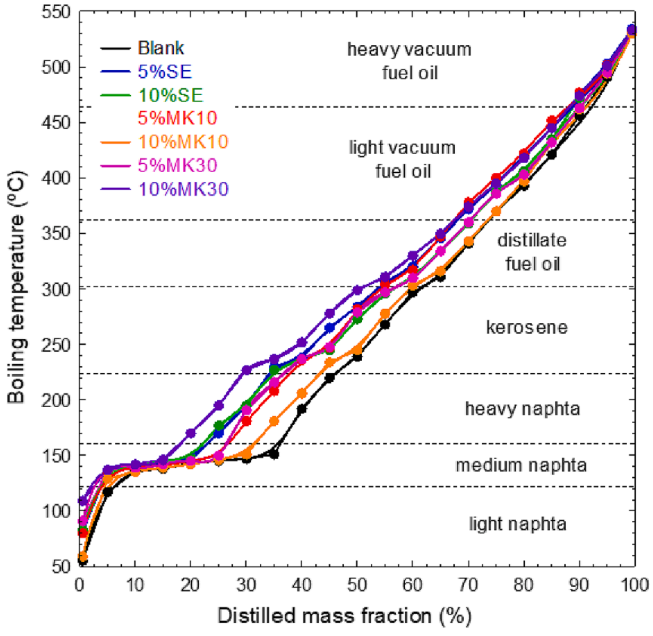

Fig. 6. Boiling temperatures as a function of the distilled mass fraction (Simulated Distillation) of the liquid fraction obtained by noncatalytic and catalytic cracking. Experimental conditions: 20 g of sample; catalyst (if added), 1 g (5% mass) or 2 g (10% mass); heating rate, 10 °C/min, holding temperature, 500 °C; holding time, 60 min; N_2 flowrate 0.8 L/min.

higher autoignition temperatures and increase octane and energy content [23,49]. The obtained gasoline does not comply with the low-temperature evaporation range according to 228 European Standard [49], and aromatic and paraffins are over specification hence could be considered like base naphtha and form part of the gasoline pool for blending with low-octane number naphtha [50–52].

Table 4
Products distribution.

Catalyst percentage in the waste plastic feed	Light Naphtha (wt.%)	Medium Naphtha (wt.%)	Heavy Naphtha (wt.%)	kerosine (wt.%)	Distillate Fuel Oil (wt.%)	Light Vacuum Gas Oil (wt.%)	Heavy Vacuum Gas Oil (wt.%)
0%	2.2	3.8	33.9	16.6	13.9	19.4	10.2
5% SE	–	3.8	25.5	18.9	16.3	22.2	13.3
10% SE	–	3.7	25.3	22.0	15.9	20.8	12.3
5% MK10	–	3.9	28.1	17.4	15.1	21.1	14.4
10% MK10	1.8	2.7	32.6	17.7	15.2	18.8	11.2
5% MK30	–	3.4	26.5	19.8	17.0	22.0	11.3
10% MK30	–	2.4	21.8	20.6	18.5	23.4	13.3

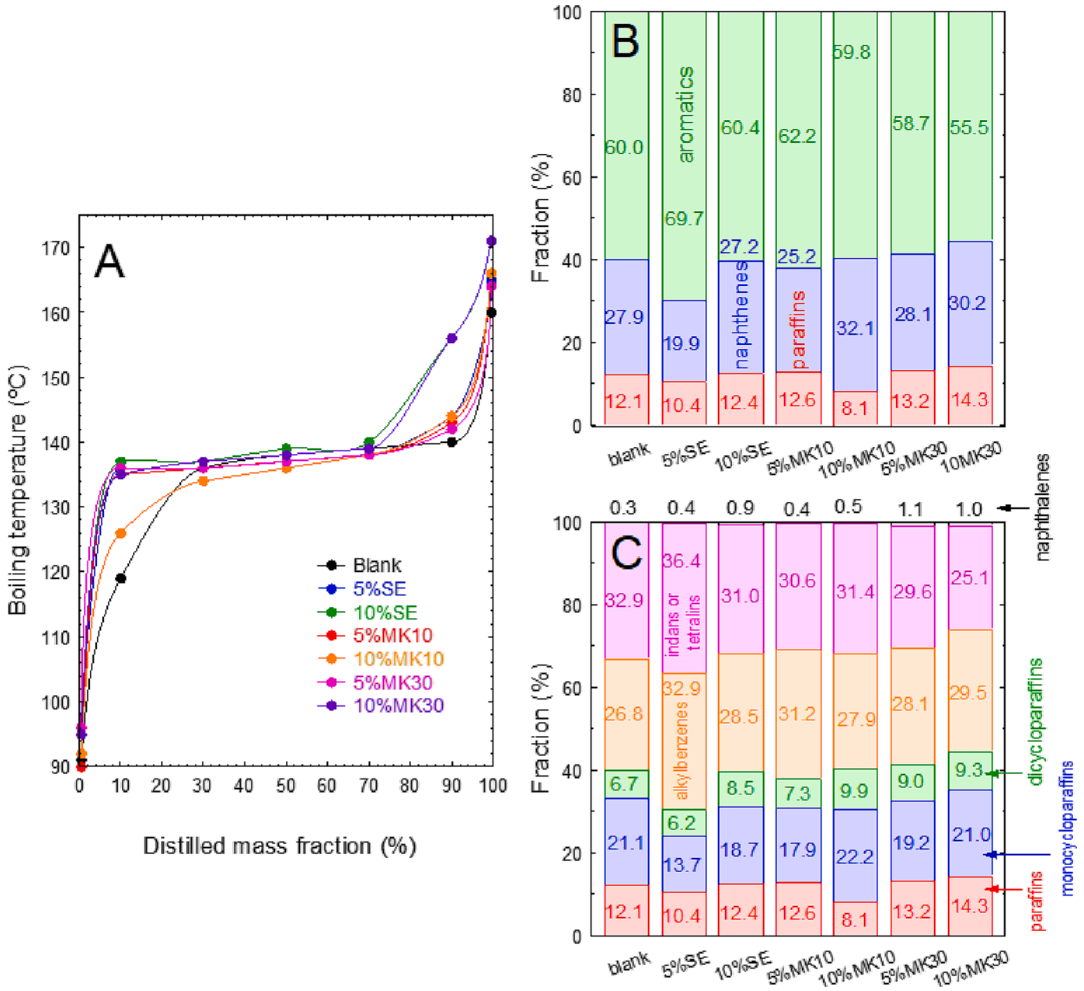

Fig. 7. ASTM D86 distillation curve (A) Hydrocarbon group (B) and the hydrocarbon types (C) distributions from gasoline cut of the liquid fraction obtained by noncatalytic and catalytic cracking. Experimental conditions: 20 g of sample; catalyst (if added), 1 g (5% mass) or 2 g (10% mass); heating rate, 10 °C/min, holding temperature, 500 °C; holding time, 60 min; N_2 flowrate 0.8 L/min.

3.4.2. Kerosine

Making the analogy with petroleum fuels, this fraction, after appropriate cleanup (sweetening treatment), is marketed as a jet fuel [51] and, for this reason, is analyzed as Jet Fuel. The ASTM D86 distillation curve for Jet Fuel (**A**), its categorization into paraffins, naphthenes, and aromatics (**B**), as well as into the types of hydrocarbon present (**C**), are shown in Fig. 8. Comparing jet fuel obtained in non-catalytic cracking of thermal cracking, the catalytic materials increase the aromaticity reducing paraffins and naphthenes of the product, which is reflected in the distillation curves.

Straight-chain paraffins are the most critical molecules of the hydrocarbons normally in jet fuel since an amount of 8–10% forms a wax crystal matrix at low temperatures; in addition, microorganisms prefer to metabolize in these (C_{12} and higher ranges); nevertheless, provide the cleanest burning while aromatics do not. Double-ring aromatics or naphthalenes have poor combustion, so the total amount of aromatics is about 25% with $\leq$ 3 %vol of naphthalenes [40,23,52]. The volatility temperature at 10% distillation of the kerosine produced is over of range required [23], except that obtained by 10% MK10, and could be corrected by modifying the end distillation point of gasoline. Nevertheless, although aromatics and naphthalenes are below the specification requirement for Jet Fuel, even if the distillation requirement is met, paraffins will still be above the limit; they cannot be used as this fuel. At the boundaries of the boiling points considered in this study, since the

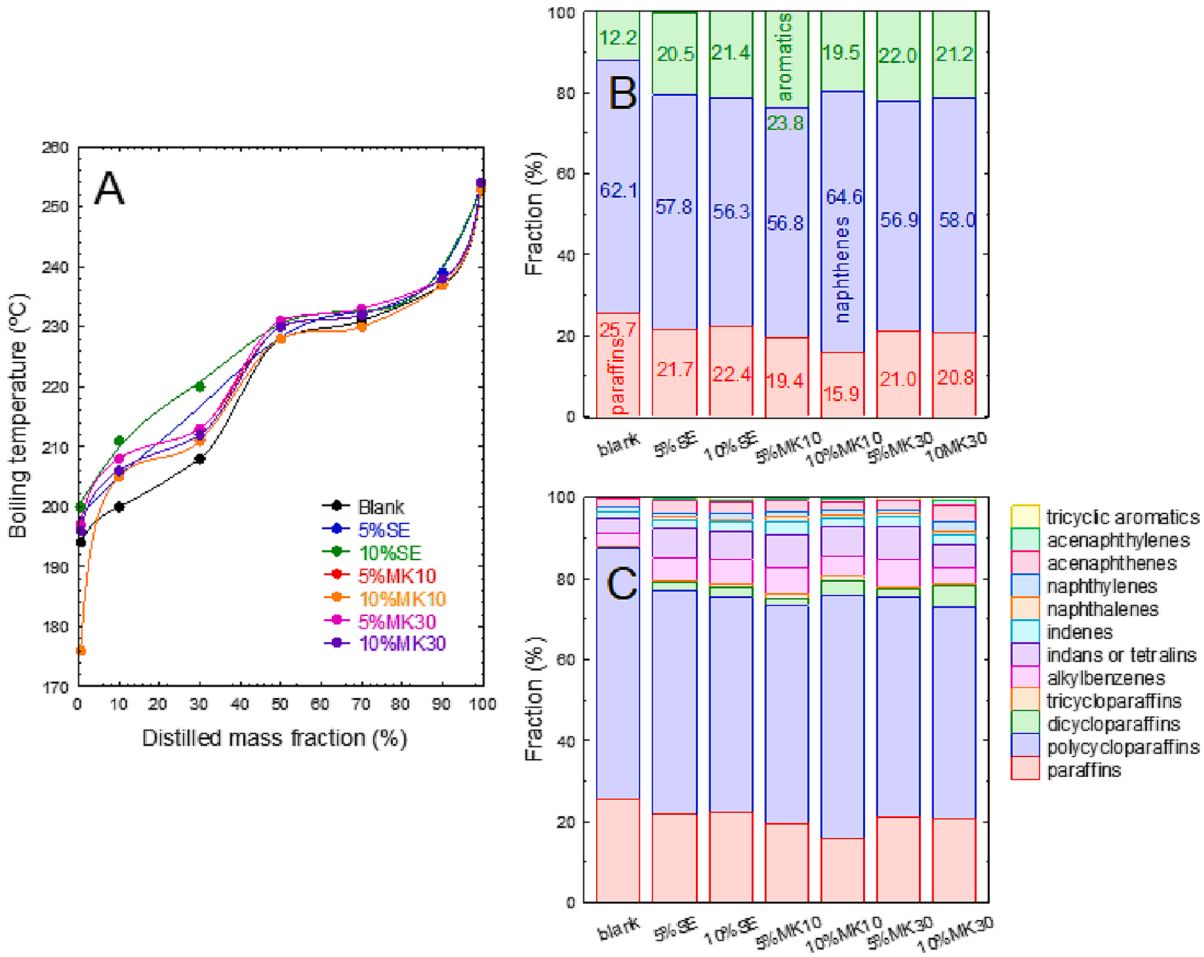

Fig. 8. ASTM D86 distillation curve (A) Hydrocarbon group (B) and the hydrocarbon types (C) distributions from kerosine cut as Jet Fuel of the liquid fraction obtained by noncatalytic and catalytic cracking. Experimental conditions: 20 g of sample; catalyst (if added), 1 g (5% mass) or 2 g (10% mass); heating rate, 10 °C/min, holding temperature, 500 °C; holding time, 60 min; N_2 flowrate 0.8 L/min.

saturated hydrocarbon derivatives of kerosine are desirable, they could be used as starting material for the production of petrochemical intermediates and the direct output of petrochemical products [53].

3.4.3. Diesel

By analogy with fossil fuels, the distillate fuel oil was analyzed as a diesel product through to its ASTM D86 distillation curve (Fig. 9**A**) and its categorization into hydrocarbon groups (paraffins, naphthenes, and aromatics Fig. 9B) together with a detailed hydrocarbon type survey (Fig. 9C**).** Compared to the diesel product obtained by noncatalytic cracking or thermal cracking, aromatic hydrocarbon increased along with a bit of paraffins by naphthenes reduction when the catalyst amount rose, except on 10% MK10, where naphthenes increase. As a result, little difference among ASTM D86 distillation curves is displayed.

Paraffins (aliphatic hydrocarbon, 64%) contribute majoritarian to fuel cetane number (decreases from n-paraffins to i-paraffins to n-olefins to i-olefins to naphthenes and aromatics); however, straight-chain paraffins supply a ignite readily under compression. In contrast, branched paraffins and aromatics react more slowly. Although aromatics have a negative impact on emissions and cetane index, they contribute to the lubrication properties, so the maximum allowed total aromatics is 10–35% (alkylbenzenes and 2-ring, 3-ring aromatics derivatives of 35% v/v, and less than 8 % m/m of polycyclic aromatics) [23,49,53]. Although the catalytic materials have an excellent performance in producing diesel due to the distillation requirements according to 590 European Standard, their polyaromatic content would not allow them to be considered as such [49].

3.4.4. Bottoms

As with the VGO of petroleum, light and heavy gas oils were analyzed together as bottoms, a semi-finished product usually processed in the fluid catalytic cracking unit (FCCU) in a refining process [53]. Fig. 10A shows this fraction classified into paraffins, naphthenes, and aromatics, while Fig. 10B shows detailed categorization by hydrocarbon types. No significative changes were observed concerning the obtained by noncatalytic cracking; nevertheless, the presence of the catalyst increased the paraffins from about 14 to 39% with a reduction from 4 to 32% of aromatics; naphthenes increased with MK10 materials (3 to 6%) and 10% of MK30. Compared to a typic fossil feedstock of an FCCU (23.9% paraffins, 37.8% cycloparaffins, 15% monoaromatics, 8.9 % diaromatics, 7.9% of polyaromatics, 5% of others [54]), all fraction has low paraffinic, high cycloparaffins, and aromatics totals amounts, the last is an acid coke precursor [37] so that these fractions could be processed in FCC unit by blending with traditional feed.

4. Conclusions

A study of the potential of a catalytic pyrolysis process to valorize plastic wastes of the rejected fractions of Granada's mechanical biological treatment plant has been carried out. A complete analysis of the products focuses on identifying and classifying the fuel fractions taking as references the fractions commonly obtained in oil refining processes (such as gasoline, kerosene, diesel, etc.).

Sepiolite and montmorillonites were used as catalysts. The commercial materials were subjected to a simple heat treatment to obtain

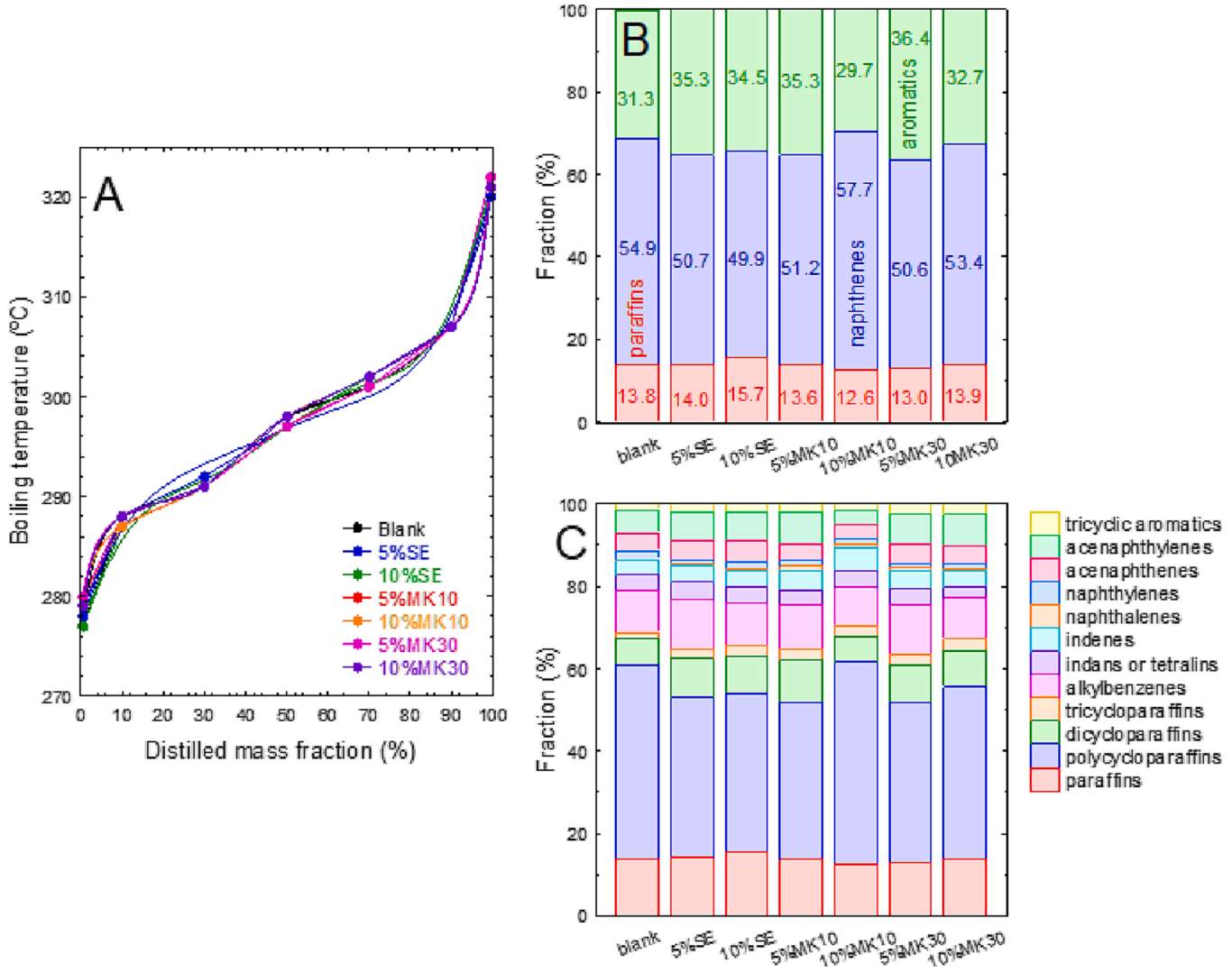

Fig. 9. ASTM D86 distillation curve (A) Hydrocarbon group (B) and the hydrocarbon types (C) distributions from distillate fuel oil cut as a diesel of the liquid fraction obtained by noncatalytic and catalytic cracking. Experimental conditions: 20 g of sample; catalyst (if added), 1 g (5% mass) or 2 g (10% mass); heating rate, 10 °C/min, holding temperature, 500 °C; holding time, 60 min; N_2 flowrate 0.8 L/min. Fig. 10. Hydrocarbon group (A) and the hydrocarbon types (B) distributions from gas oil cuts as bottoms of the liquid fraction obtained by noncatalytic and catalytic cracking.

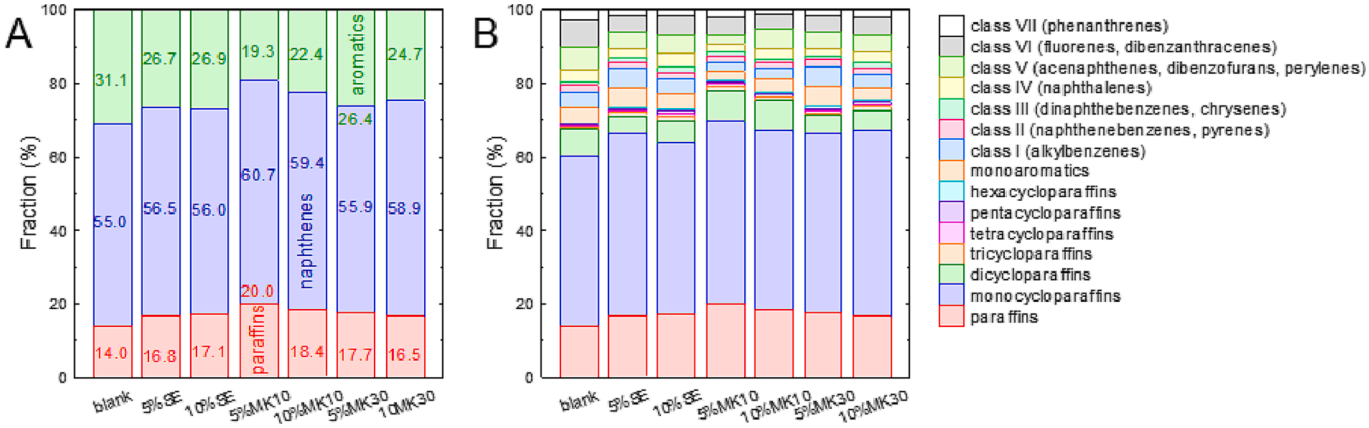

Fig. 10. Hydrocarbon group (A) and the hydrocarbon types (B) distributions from gas oil cuts as bottoms of the liquid fraction obtained by noncatalytic and catalytic cracking.

samples with a well-defined porous structure and advantageous acidity properties for the catalytic step. Montmorillonites exhibited NH_3-TPD with a dominant peak associated with weak acid sites, while sepiolite displayed acid sites of greater strength and a broad band with a maximum located at 315 ^{o}C. The analysis of a combined morphologic/acidity parameter provides a quantitative conclusion that confirms that higher liquid fraction can be optimized using Montmorillonites with high surface area and weak acid sites. The porous distribution also showed a clear influence on the yield products.

The results indicate that the volatilization temperature of the liquid products obtained from catalytic cracking increased due to changes in the product distribution, which were caused by a substantial rise in gas yield, up to 20 wt%. This increase in gas yield can be attributed to the thermal cracking of light compounds within the liquid fraction, leading to a reduction in their concentration from 4 to 11 wt%.

A remarkably higher amount of high boiling cuts was detected, which increased from 5 to 42 wt%. The leftward shift of the distillation curves indicates a decrease in naphtha by up to 36 wt%, while kerosene experienced a rise of 32 wt%.

Distillate fuel oil showed an increase of 33%, and both light and heavy vacuum gas oils exhibited a rise of 21% and 41%, respectively, compared to thermal cracking conditions.

A full screening of gasoline, kerosine, diesel, and bottoms, by analogy with hydrocarbon present in petroleum, was carried out by Simulated Distillations. At optimized operating conditions, the process could allow obtaining liquid.

This approach critically assesses the potential of a thermal-catalytic valorization scheme for real plastic waste in the current energy context, which is still dominated by fuels derived from the petroleum industry. The assessment is based on a strict analysis of the fractions using Simulated Distillation.

At optimized operating conditions, the process could allow obtaining liquid products which can be part of the gasoline pool for blending with low-octane number naphtha, a fraction with similar properties to the diesel fraction, a kerosene fraction to be used as starting material for the production of petrochemical or the commonly called button fraction products with properties similar to the vacuum gas oil of petroleum industry (light and heavy gas oils) which could be processed in FCC units.

The approach situates, with a critical perspective and based on a strict analysis of the fractions by Simulated Distillation, the potential of a thermal-catalytic valorization scheme of real plastic solid waste in the current energy context, which is still dominated by the fuels generated by petroleum industry.

Declaration of Competing Interest

The authors declare that they have no known competing financial interests or personal relationships that could have appeared to influence the work reported in this paper.

Data availability

Data will be made available on request.

Acknowledgements

This work has received funds from the project PID2019-108826RB-I00/SRA (State Research Agency)/10.13039/501100011033 and the project B-RNM-78-UGR20 (FEDER/Junta de Andalucía-Ministry of Economic Transformation, Industry, and Universities). Funding for open access charge: Universidad de Granada / CBUA.

Appendix A. Supplementary data

Supplementary data to this article can be found online at https://doi.org/10.1016/j.fuel.2023.129145.

References

[1] Anuar Sharuddin SD, Abnisa F, Wan Daud WMA, Aroua MK. A review on pyrolysis of plastic wastes. Energy Convers Manag 2016;115:308–26. https://doi.org/10.1016/j.enconman.2016.02.037.
[2] M. S. Qureshi *et al.*, "Pyrolysis of plastic waste: Opportunities and challenges," *J. Anal. Appl. Pyrolysis*, vol. 152, no. February, 2020, doi: 10.1016/j.jaap.2020.104804.
[3] Gebre SH, Sendeku MG, Bahri M. Recent Trends in the Pyrolysis of Non-Degradable Waste Plastics. ChemistryOpen 2021;10(12):1202–26. https://doi.org/10.1002/open.202100184.
[4] Schwarz AE, Ligthart TN, Godoi Bizarro D, De Wild P, Vreugdenhil B, van Harmelen T. Plastic recycling in a circular economy; determining environmental performance through an LCA matrix model approach. Waste Manag 2021;121:331–42. https://doi.org/10.1016/j.wasman.2020.12.020.
[5] Budsaereechai S, Hunt AJ, Ngernyen Y. Catalytic pyrolysis of plastic waste for the production of liquid fuels for engines. RSC Adv 2019;9(10):5844–57. https://doi.org/10.1039/c8ra10058f.
[6] Quesada L, Pérez A, Godoy V, Peula FJ, Calero M, Blázquez G. Optimization of the pyrolysis process of a plastic waste to obtain a liquid fuel using different mathematical models. Energy Convers Manag 2019;188(March):19–26. https://doi.org/10.1016/j.enconman.2019.03.054.
[7] Paucar-Sánchez MF, Calero M, Blázquez G, Solís RR, Muñoz-Batista MJ, Martín-Lara MÁ. Thermal and catalytic pyrolysis of a real mixture of post-consumer plastic waste: An analysis of the gasoline-range product. Process Saf Environ Prot 2022;168(October):1201–11. https://doi.org/10.1016/j.psep.2022.11.009.
[8] R. R. Solís, M. Á. Martín-Lara, A. Ligero, J. Balbís, G. Blázquez, and M. Calero, "Revalorizing a Pyrolytic Char Residue from Post-Consumer Plastics into Activated Carbon for the Adsorption of Lead in Water," *Appl. Sci.*, vol. 12, no. 16, 2022, doi: 10.3390/app12168032.
[9] D. A. Wijesekara, P. Sargent, C. J. Ennis, and D. Hughes, "Prospects of using chars derived from mixed post waste plastic pyrolysis in civil engineering applications," *J. Clean. Prod.*, vol. 317, no. December 2020, p. 128212, 2021, doi: 10.1016/j.jclepro.2021.128212.
[10] Harussani MM, Sapuan SM, Rashid U, Khalina A, Ilyas RA. Pyrolysis of polypropylene plastic waste into carbonaceous char: Priority of plastic waste management amidst COVID-19 pandemic. Sci Total Environ 2022;803. https://doi.org/10.1016/j.scitotenv.2021.149911.
[11] Parrilla-Lahoz S, et al. Materials challenges and opportunities to address growing micro/nanoplastics pollution: a review of thermochemical upcycling. Mater Today Sustain 2022;20. https://doi.org/10.1016/j.mtsust.2022.100200.
[12] Al-Salem SM, Antelava A, Constantinou A, Manos G, Dutta A. A review on thermal and catalytic pyrolysis of plastic solid waste (PSW). J Environ Manage 2017;197(1408):177–98. https://doi.org/10.1016/j.jenvman.2017.03.084.
[13] Miandad R, Barakat MA, Aburiazaiza AS, Rehan M, Nizami AS. Catalytic pyrolysis of plastic waste: A review. Process Saf Environ Prot 2016;102:822–38. https://doi.org/10.1016/j.psep.2016.06.022.
[14] Y. Peng *et al.*, "A review on catalytic pyrolysis of plastic wastes to high-value products," *Energy Convers. Manag.*, vol. 254, no. December 2021, p. 115243, 2022, doi: 10.1016/j.enconman.2022.115243.
[15] Dai L, et al. Pyrolysis technology for plastic waste recycling: A state-of-the-art review. Prog Energy Combust Sci 2022;vol. 93, no. June. https://doi.org/10.1016/j.pecs.2022.101021.
[16] Wang K, Johnston PA, Brown RC. Comparison of in-situ and ex-situ catalytic pyrolysis in a micro-reactor system. Bioresour Technol 2015;173:124–31. https://doi.org/10.1016/j.biortech.2014.09.097.
[17] American Society for Testing and Materials, "Surface Area of Catalysts and Catalyst Carriers," ASTM Int., vol. 05, no. Reapproved, pp. 1–5, 2007.
[18] American Society for Testing and Materials, "Standard Test Method for Determining Micropore Volume and Zeolite Area of a," ASTM Int., vol. 05, no. Reapproved, pp. 1–6, 2001.
[19] American Society for Testing and Materials, "Standard Practice for Calculation of Pore Size Distributions of Catalysts from," ASTM Int., vol. 94, no. Reapproved 2006, pp. 1–6, 2012, doi: 10.1520/D4641-17.2.
[20] American Society for Testing and Materials, "Standard Test Methods for Instrumental Determination of Carbon, Hydrogen, and Nitrogen in Petroleum Products and Lubricants," Man. Hydrocarb. Anal. 6th Ed., pp. 852-852–5, 2008, doi: 10.1520/mnl10969m.
[21] American Society for Testing and Materials, "Standard Test Method for Boiling Range Distribution of Petroleum Fractions by Gas Chromatography," ASTM International. p. 20, 2008.
[22] Montemayor RG. Distillation and Vapor Pressure Measurement in Petroleum Products. West Conshohocken: ASTM International; 2008.
[23] Totten G, Westbrook S, Shah R. Fuels and Lubricants Handbook: Technology, Properties, Performance, and Testing, ASTM. Glen Burnie: ASTM International; 2003.
[24] American Petroleum Institute. Technical Data Book American Petroleum Institute. American Petroleum Institute; 1999.
[25] American Society for Testing and Materials, "Standard Test Method for Hydrocarbon Types in Low Olefinic Gasoline by Mass Spectrometry," ASTM Int., vol. i, no. Reapproved 2016, pp. 1–7, 2013.

[26] American Society for Testing and Materials, "Standard Test Method for Hydrocarbon Types Analysis of Gas-Oil Saturates Fractions by High Ionizing Voltage Mass Spectrometry," ASTM Int., no. Reapproved 2016, pp. 1–8, 1991.
[27] American Society for Testing and Materials, "Standard Test Method for Aromatic Types Analysis of Gas-Oil Aromatic Fractions by High Ionizing Voltage Mass Spectrometry," ASTM Int., no. Reapproved 2016, pp. 1–15, 1991.
[28] American Society for Testing and Materials, "Standard Test Method for Hydrocarbon Types in Middle Distillates by Mass," vol. i, no. Reapproved 2009, pp. 1–6, 2013, doi: 10.1520/D2789-05R16.2.
[29] Thommes M, et al. Physisorption of gases, with special reference to the evaluation of surface area and pore size distribution (IUPAC Technical Report). Pure Appl Chem 2015;87(9–10):1051–69. https://doi.org/10.1515/pac-2014-1117.
[30] Campelo JM, Garcia A, Luna D, Marinas JM. Textural properties, surface chemistry and catalytic activity in cyclohexene skeletal isomerization of acid treated natural sepiolites. Mater Chem Phys 1989;24(1–2):51–70. https://doi.org/10.1016/0254-0584(89)90045-X.
[31] Suárez M, García-Romero E. Variability of the surface properties of sepiolite. Appl Clay Sci 2012;67–68:72–82. https://doi.org/10.1016/j.clay.2012.06.003.
[32] F. W. Harun, E. A. Almadani, and S. M. Radzi, "Metal cation exchanged montmorillonite K10 (MMT K10): Surface properties and catalytic activity," *J. Sci. Res. Dev.*, vol. 3, no. 3, pp. 90–96, 2016, [Online]. Available: www.jsrad.org.
[33] Jang BS, Cho KH, Kim KH, Park DW. Degradation of polystyrene using montmorillonite clay catalysts. React Kinet Catal Lett 2005;86(1):75–82. https://doi.org/10.1007/s11144-005-0297-z.
[34] Karimi E, et al. Red mud as a catalyst for the upgrading of hemp-seed pyrolysis bio-oil. Energy Fuel 2010;24(12):6586–600. https://doi.org/10.1021/ef101154d.
[35] Chen M, et al. Hydrogen production by ethanol steam reforming over M-Ni/sepiolite (M = La, Mg or Ca) catalysts. Int J Hydrogen Energy 2021;46(42):21796–811. https://doi.org/10.1016/j.ijhydene.2021.04.012.
[36] Zhang J, et al. Catalytic Cracking of n-Decane over Monometallic and Bimetallic Pt-Ni/MoO 3 /La-Al 2 O 3 Catalysts: Correlations of Surface Properties and Catalytic Behaviors. Ind Eng Chem Res 2019;58(5):1823–33. https://doi.org/10.1021/acs.iecr.8b04712.
[37] Richardson JT. Principles of Catalyst Development, Second Pri. New York: Springer Science+Business Media, LLC; 1992.
[38] Zhou CH, et al. Roles of texture and acidity of acid-activated sepiolite catalysts in gas-phase catalytic dehydration of glycerol to acrolein. Mol Catal 2017;434:219–31. https://doi.org/10.1016/j.mcat.2016.12.022.
[39] Pérez Pariente J, Fornés V, Corma A, Mifsud A. The surface acidity and hydrothermal stability of sepiolite derivatives. Appl Clay Sci 1988;3(4):299–306. https://doi.org/10.1016/0169-1317(88)90021-X.
[40] P. (IFP) Wuithier, Le Pétrole REFFINAGE ET GÈNIE CHIMIQUE, Tome 1, 2nd ed. Paris: Technip, 1972.
[41] L. Quesada, M. Calero, M. Á. Martín-Lara, A. Pérez, M. F. Paucar-Sánchez, and G. Blázquez, "Characterization of the Different Oils Obtained through the Catalytic In Situ Pyrolysis of Polyethylene Film from Municipal Solid Waste," *Appl. Sci.*, vol. 12, no. 8, 2022, doi: 10.3390/app12084043.
[42] M. R. Riazi, Characterization and Properties of Petroleum Fractions, 1st ed., vol. 1, no. 1. Philadelphia: ASTM, 2005.
[43] Speight JG. The Chemistry and Technology of Petroleum, Fourth. Boca Raton: CRC Press; 2006.
[44] B. C. Smith, *Infrared Spectral Interpretation: a systematic approach*, vol. 3, no. April. Boca Raton: CRC Press, 1999.
[45] Kusenberg M, et al. A comprehensive experimental investigation of plastic waste pyrolysis oil quality and its dependence on the plastic waste composition. Fuel Process Technol 2022;227(November). https://doi.org/10.1016/j.fuproc.2021.107090.
[46] Bauserman JW, Mushrush GW, Hardy DR. Organic nitrogen compounds and fuel instability in middle distillate fuels. Ind Eng Chem Res 2008;47(9):2867–75. https://doi.org/10.1021/ie071321n.
[47] P. Schempp, S. Köhler, M. Menzebach, K. Preuss, and M. Tröger, "Corrosion in the crude distillation unit overhead line: Contributors and solutions," *EUROCORR 2017 - Annu. Congr. Eur. Fed. Corros. 20th Int. Corros. Congr. Process Saf. Congr. 2017*, no. September, 2017.
[48] C. G. Cárdenas, B., "Analysis of the acid number of crude oils with different API gravity and their typical fractions," National Polytechnic Institute of Mexico, 2015.
[49] B. O. del E. (BOE), Real Decreto 1088/2010 por el que se modifica el Real Decreto 61/2006, de 31 de enero, en lo relativo a las especificaciones técnicas de gasolinas, gasóleos, utilización de biocarburantes y contenido de azufre de los combustibles para uso marítimo. Madrid: Agencia Estatal Boletín Oficial del Estado, 2010.
[50] Rahimpour MR, Jafari M, Iranshahi D. Progress in catalytic naphtha reforming process: A review. Appl Energy 2013;109:79–93. https://doi.org/10.1016/j.apenergy.2013.03.080.
[51] Meyers RA. Handbook of Petroleum Refining Processes. Third: Second; 2004.
[52] J.-P. (IFP) Wauquier, *El Refino Del Petróleo*. Madrid: Díaz de Santos - ISE, 2004.
[53] Speight JG. Handbook of Petrochemical Processes. Boca Raton: CRC Press; 2019.
[54] Ng SH. Conversion of Polyethylene Blended with VGO to Transportation Fuels by Catalytic Cracking. Energy Fuel 1995;9(2):216–24. https://doi.org/10.1021/ef00050a003.